Pump Probe Scheme To Study the Autoionization Decay of Optically-Forbidden H-2 Doubly Excited States

ARTICLE *in* THE JOURNAL OF PHYSICAL CHEMISTRY A · AUGUST 2012

Impact Factor: 2.69 · DOI: 10.1021/jp3053136 · Source: PubMed

3 AUTHORS, INCLUDING:

Rui Silva
Universidad Autónoma de Madrid
5 PUBLICATIONS **40** CITATIONS

THE JOURNAL OF PHYSICAL CHEMISTRY A

Article

pubs.acs.org/JPCA

Pump−Probe Scheme To Study the Autoionization Decay of Optically-Forbidden H_2 Doubly Excited States

P. Rivière,*[,†] R. E. F. Silva,[†] and F. Martín[†,‡]

[†]Departamento de Química, Módulo 13, Universidad Autónoma de Madrid, 28049 Madrid, Spain,and

[‡]Instituto Madrileño de Estudios Avanzados en Nanociencia, Cantoblanco, 28049 Madrid, Spain

ABSTRACT: A pump−probe scheme is proposed to investigate the autoionization dynamics of the optically forbidden $Q_1{}^1\Sigma_g^+$ doubly excited states of the H_2 molecule. The scheme consists of a pump that contains an attosecond pulse train (APT) and an infrared (IR) pulse, which is phase-locked with the APT, and an IR probe identical to the former IR pulse. The dynamical information is obtained by analyzing the electron kinetic energy spectra (EKE) and proton kinetic energy spectra (PKE) as a function of the time delay between the pump and the probe. The essential requirement for an efficient population of the $Q_1{}^1\Sigma_g^+$ states is that they are resonantly coupled to both the dipole-allowed $Q_1{}^1\Sigma_u^+$ doubly excited states and the ground state of H_2 by the combined effect of the APT + IR fields.

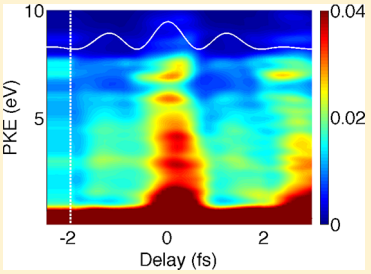

1. INTRODUCTION

In the past decade we have witnessed a revolution in the generation of ultrashort laser pulses. Nowadays a full collection of laser sources, including phase-stable femtosecond infrared pulses, as well as single attosecond pulses and attosecond pulse trains, is available to perform experiments on atomic and molecular systems with femto- and attosecond time resolution.[1−4] In particular, they can be used to study molecular autoionization,[5] because this process typically occurs in the femtosecond time scale (see, e.g., refs 6, 7, and 24 and references therein).

Autoionization is a process triggered by electron correlation. It occurs when two or more valence electrons are excited and one of them is spontaneously ejected in the continuum, or when one inner-shell electron is missing, in which case an electron from an upper shell occupies the hole and another electron is ejected (Auger effect). Autoionization has been used to track fast electron dynamics in atoms and to characterize X-ray pulses.[8−12] In molecules, the investigation of electron dynamics is substantially more complicated than in atoms because autoionization lifetimes are typically of the same order of magnitude as the molecular vibrational period or the time for molecular dissociation. Hence, the nuclei have enough time to move, even outside the Franck−Condon (FC) region, before the electron is ejected, so that the classical picture in which the nuclei remain static during electron emission is not valid any more.[13−16] As a consequence, a time-dependent theoretical treatment of molecular autoionization is considerably more involved: it must not only describe electron correlation properly but also account for the nuclear motion, and all this in a fully quantum mechanical manner because autoionization and direct ionization may also interfere as a result of the wave-like behavior of both electrons and nuclei.[13,14] Such a sophisticated theoretical treatment is only accessible for the simplest molecular system, H_2 (or D_2). The method used in this work, which satisfies the former requirements, has been recently proposed and adapted to treat autoionization.[17−19]

The H_2 molecule possesses different series of doubly excited states (DESs), which are embedded in and coupled to the electronic continuum through electron correlation.[20,21] All these states have repulsive potential energy curves that lead to dissociation. These states can either dissociate into neutral (H + H) or ionic ($H^+ + H^-$) fragments or autoionize, nondissociatively ($H_2^{**} \rightarrow H_2^+ + e^-$) or dissociatively ($H_2^{**} \rightarrow H^+ + H + e^-$).

Autoionization lifetimes in atoms can be inferred from the autoionization widths in electronic spectra. However, in molecules, nuclear motion significantly affects the interferences among the different decay channels, thus preventing one from obtaining such autoionization widths from a simple fit of the measured spectra. For this reason, most properties of the DESs of the H_2 molecule have been obtained from theoretical works (see, e.g., refs 23 and 24). Autoionizing states play an important role as intermediate states in single- and multiphoton absorption, electron impact excitation, associative ionization and $e^- + H_2^+$ scattering (see ref 24 and references therein).

Different schemes have been used to study H_2 autoionization with ultrashort laser pulses: one-photon XUV photoionization (see refs 14 and 25 and references therein) and pump−probe setups like XUV-pump/XUV-probe[26,27] and XUV-pump/IR-probe.[5] The latter pump−probe schemes have been implemented with single femto- or attosecond pulses. An alternative is to use attosecond pulse trains (APT) in an APT-pump/IR-probe scheme.[28,29] The advantage of attosecond pulse trains with respect to single attosecond pulses, apart from being easier to produce experimentally, is that their energy spectrum consists of narrow peaks (∼1 eV). Due to their short duration they allow us to explore electron dynamics in a subfs time scale,

Special Issue: Jörn Manz Festschrift

Received: May 31, 2012
Revised: July 12, 2012

   dx.doi.org/10.1021/jp3053136 | J. Phys. Chem. A XXXX, XXX, XXX−XXX

and due to their spectral selectivity, only specific bands of states are populated.

By using the schemes reported above, only DESs populated by optically allowed transitions can be investigated. For the H_2 molecule, these are the $^1\Sigma_u^+$ and $^1\Pi_u$ DESs. The reason is that, in general, XUV pump pulses are weak and, therefore, population of the DESs by absorption of a single photon is entirely dictated by the dipole selection rule. The latter rule imposes restrictions to the symmetry of the final states, which, for the case of H_2 initially in the $X^1\Sigma_g^+$ ground state, can only be $^1\Sigma_u^+$ and $^1\Pi_u$. A work on the dynamics of the $Q_1{}^1\Sigma_u^+$ states has been recently published,[29] in which the strong effect of such DESs on the proton kinetic energy spectra is discussed. In that work, an APT-pump−IR-probe scheme has been used, in which an XUV photon from the APT populates the DESs that are later probed with the IR field. A similar strategy does not work for $^1\Sigma_g^+$ doubly excited states because one-photon transitions from the $X^1\Sigma_g^+$ ground state are forbidden by the dipole selection rule. Thus, traditionally, the dynamics of the $^1\Sigma_g^+$ doubly excited states has been investigated in collisions of slow electrons with H_2. In these collisions, the dipole selection rule does not apply and states of any final symmetry can in principle be populated. However, due to the broad energy band associated with this kind of collisions, selectivity is very small and a large number of states of different symmetries is populated, thus complicating the analysis. Increasing the energy of the impinging electron improves selectivity, but then optically allowed dipole transitions become dominant and, consequently, are not suitable to investigate the autoionization dynamics of the $^1\Sigma_g^+$ states.[22]

The $^1\Sigma_g^+$ doubly excited states can also be populated by absorption of an even number of photons. Although multiphoton absorption is in general less efficient than single-photon absorption, selectivity is much larger than in electron−H_2 collisions. Thus $^1\Sigma_g^+$ doubly excited states could be reached from the ground state by absorption of, e.g., two identical photons of about ∼14 eV. However, absorption of the first photon is resonantly coupled to the $^1\Sigma_u^+$ and $^1\Pi_u$ singly excited states of H_2[27] and, therefore, the nuclear wave packet dynamics that is induced in these intermediate states might hinder the analysis of the autoionization decay that occurs after absorption of the second photon.

An alternative approach is the use of a pump formed by a XUV-APT phase locked to an IR pulse, in which the XUV photons have enough energy to go above the ionization threshold (thus avoiding the bound-state region) and the energy resulting from the combination of the XUV and IR photons is resonant with one of the $Q_1{}^1\Sigma_g^+$ doubly excited states. The autoionizing decay of these states can thus be probed by using another IR pulse whose delay with the former pump can be varied at will. Such an (APT+IR)-pump/IR-probe scheme has recently been implemented in the laboratory.[10,30]

In this work we investigate the autoionization dynamics of the optically forbidden $Q_1{}^1\Sigma_g^+$ DESs of H_2. The pump−probe setup is designed to maximize the population of such states through a resonance enhanced two-photon transition. The pump consists of an attosecond pulse train that is phase-locked to an IR field of frequency ω. The most intense harmonic of the APT is tuned to the energy difference between the ground state of the molecule and the lowest $Q_1{}^1\Sigma_u^+$ DES (Figure 1). This is the harmonic 19th of the IR generating field, which we will denote H19. Emission of an IR photon can resonantly populate the lowest $Q_1{}^1\Sigma_g^+$ state, through the process

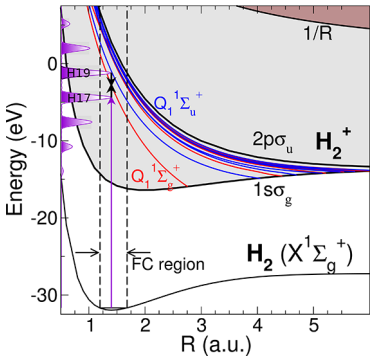

Figure 1. Born−Oppenheimer potential energy curves of the H_2 and H_2^+ molecules. The energy spectrum of the APT is depicted in purple. The gray zone corresponds to ionization, and the Franck−Condon region lies between the vertical dashed lines. The vertical arrows represent the absorption of an XUV photon (purple) and absorption or emission of IR photons (black) from the H_2 ground state at the equilibrium distance (R = 1.4 au). The red and blue curves represent the $Q_1{}^1\Sigma_g^+$ and $Q_1{}^1\Sigma_u^+$Q DESs, respectively.

$$X^1\Sigma_g^+ \xrightarrow{+H19} 1Q_1{}^1\Sigma_u^+ \xrightarrow{-\omega} 1Q_1{}^1\Sigma_g^+ \tag{1}$$

Alternatively, the DES can be accessed after absorption of a smaller XUV photon,

$$X^1\Sigma_g^+ \xrightarrow{+H17+\omega} 1Q_1{}^1\Sigma_g^+ \tag{2}$$

The probe is another IR field, of the same frequency and intensity as those of the pump IR. All fields are linearly polarized in the direction of the internuclear axis. Within this scheme, the time delay between the pump and the probe will be changed to explore the autoionization dynamics.

The paper is organized as follows: the theoretical method is described in section section 2. Results are shown in section 3, in particular photoelectron spectra (section 3.1) and proton kinetic energy release spectra (section 3.2). Some conclusions are drawn in section 4. Atomic units are used throughout unless otherwise specified.

2. THEORETICAL FRAMEWORK

We summarize here the basic ingredients of the method, which has been explained in detail in refs 17−19. We solve the time-dependent Schrödinger equation (TDSE)

$$\left[\hat{H}_0(\mathbf{r},R) + \hat{V}(t) - i\frac{\partial}{\partial t}\right]\Phi(\mathbf{r},R,t) = 0 \tag{3}$$

where $\mathbf{r}$ represents the electronic coordinates $\mathbf{r}_1$ and $\mathbf{r}_2$ and R is the internuclear distance. $\hat{H}_0$ is the field-free nonrelativistic Hamiltonian of the H_2 molecule,

$$\hat{H}_0(\mathbf{r},R) = \hat{T}(R) + \hat{H}_{el}(\mathbf{r},R) \tag{4}$$

where $\hat{T}(R) = -\hat{\nabla}_R^2/2\mu$ is the relative kinetic energy of the nuclei, μ is the reduced mass, and $\hat{H}_{el}(\mathbf{r},R)$ is the electronic Hamiltonian, which includes the $1/R$ repulsion term. Mass polarization terms and relativistic effects are neglected.

The Feshbach formalism is used to deal with autoionization.[21] Within this formalism, two orthogonal complementary subspaces P and $Q = 1 - P$ are defined, with associated projectors $\hat{P}$ and $\hat{Q}$. The total wave function $\Phi(r,R,t)$ is expanded on the basis

dx.doi.org/10.1021/jp3053136 | J. Phys. Chem. A XXXX, XXX, XXX−XXX

of molecular eigenstates associated with each subspace, which are not eigenstates of the molecular Hamiltonian, and thus they are coupled in the TDSE. This basis consists of a set of vibronic stationary states, which are products of an electronic wave function and a vibrational or dissociative wave function.[31] The expansion includes three kinds of electronic wave functions: bound states, resonant states, and continuum states, calculated in a dense enough grid of internuclear distances.[18] The bound and resonant states are obtained from configuration interaction calculations, and continuum states are obtained from L^2 close-coupling calculations performed within a box.[14,32]

The bound states Φ_n of the H_2 molecule are eigenfunctions with eigenenergy ε_n of the electronic Hamiltonian,

$$\hat{H}_{el}(r,R)\,\Phi_n(r) = \mathcal{E}_n(R)\,\Phi_n(r) \tag{5}$$

The resonances associated with the Q subspace are eigenfunctions of the projected Hamiltonian,

$$[\hat{Q}\hat{H}_{el}\hat{Q} - \mathcal{E}_r(R)]\Psi_r(r;R) = 0 \tag{6}$$

and analogously, the nonresonant states associated with the electronic continuum in the P subspace are the solutions of

$$[\hat{P}\hat{H}_{el}\hat{P} - \mathcal{E}(R)]\Psi_\alpha^{el}(r;\,R) = 0 \tag{7}$$

$$\mathcal{E}(R) - E_\alpha(R) + \varepsilon = 0 \tag{8}$$

The full set of quantum numbers for the electronic state of the molecular ion H_2^+ with a BO energy $E_\alpha(R)$ is denoted by α, whereas ε and l are the energy and angular momentum of the ejected electron. After the electronic structure has been obtained in a given grid of internuclear distances, the nuclear one-dimensional Schrödinger equation

$$\left[-\frac{\hat{\nabla}_R^{\,2}}{2\mu} + \mathcal{E}_x(R)\right]\chi_{\nu_x}(R) = W_{\nu_x}\chi_{\nu_x}(R) \tag{9}$$

is solved, where x stands for a bound, continuum or resonant state of H_2, and W_{ν_x} is the vibronic energy associated with the x electronic state. The total wave function, including bound, resonant and continuum terms, is thus written

$$\begin{aligned}\Phi(r,R,t) = &\sum_n \sum_{\nu_n}^{f} C_{n\nu_n}(t)\,\Psi_n(r;R)\,\chi_{\nu_n}(R)e^{-iW_{\nu_n}t} \\ &+\sum_r \sum_{\nu_r}^{f} C_{r\nu_r}(t)\,\Psi_r(r;R)\,\chi_{\nu_r}(R)e^{-iW_{\nu_r}t} \\ &+\sum_{\alpha,l}\int d\varepsilon \sum_{\nu_\alpha}^{f} C^{\varepsilon l}_{\alpha,\nu_\alpha}(t)\Psi^{\varepsilon l}_\alpha(r;R)\,\chi_{\nu_\alpha}(R)e^{-iW_{\nu_\alpha}t}.\end{aligned} \tag{10}$$

Inserting eq 10 into eq 3 and projecting onto the basis of vibronic states leads to a set of coupled differential equations, where nonadiabatic couplings have been neglected. States with different symmetry are coupled by the laser potential, and the continuum and resonant states with the same symmetry are coupled by $\hat{Q}\hat{H}_{el}\hat{P}$ and $\hat{P}\hat{H}_{el}\hat{Q}$ terms. Note that the energy dependence of all matrix elements is fully taken into account. This set of equations is integrated up to $t_{max} \gg T_{AI}$, where $T_{AI} = 1/\Gamma$ is the maximum autoionization time. A simple projection of the total wave function onto the $\Psi_{k\nu_k}(r,R)$ basis states provides amplitudes that can be written in terms of the C_i expansion coefficients.

Finally, the laser potential is described in the dipole approximation and velocity gauge,

$$\hat{V}(t) = (\hat{\mathbf{p}}_1 + \hat{\mathbf{p}}_2)\cdot\hat{\mathbf{A}}(t) \tag{11}$$

where $\hat{\mathbf{p}}_i$ is the momentum operator of the i electron and $\hat{\mathbf{A}}(t)$ is the operator of the vector potential of the electromagnetic field, which is described classically.

The scheme we use to study the $Q_1{}^1\Sigma_g^+$ resonances is an (APT+IR)-pump/IR-probe setup (Figure 2), in which the two fields in the pump are phase-locked. All fields are linearly polarized, with polarization direction parallel to the internuclear axis. The APT is formed by a train of four XUV pulses with fwhm = 200 as and frequency 17ω, where ω =1.605 eV is the frequency of the generating IR field, separated by $T/2$, where T is the IR period. This leads to an energy spectrum formed by odd harmonics of the generating frequency. The corresponding energy spectrum has two principal harmonics at frequencies 17ω and 19ω (Figure 1), which we will denote H17 and H19, and the less intense harmonics H13, H15, H21, and H23. The frequency is chosen to match the energy difference between the H_2 ground rovibrational state and the first $Q_1{}^1\Sigma_u^+$ resonance. Upon emission of an IR photon, the first $Q_1{}^1\Sigma_g^+$ can be populated. The intensity of the APT is 10^9 W/cm^2 for the two central pulses and 0.35×10^9 W/cm^2 for the external pulses, which corresponds to an APT envelope with fwhm = 3 fs and $I = 1.14 \times 10^9$ W/cm^2. Both IR fields have a frequency ω = 1.605 eV, an intensity 10^{12} W/cm^2, and a duration of three cycles. The attosecond pulses of the APT are located at maxima of the phase-locked IR field, which maximizes two-photon absorption and therefore the population of the optically forbidden resonances. A scan in delays between the pump and probe is performed, where the delay Δt is defined with respect to the center of IR envelopes, and $\Delta t > 0$ means that the (APT+IR) pump comes before the IR probe. We note that, for the chosen intensity and frequency of the IR fields, the maximum value of the ponderomotive energy when both IR fields interfere constructively is U_p = 0.11 eV, which is much smaller than the bandwidth of the XUV harmonics and the IR fields. Therefore, the effect of the IR field on the potential curves of the Q_1 doubly excited states and on their population will be barely visible.

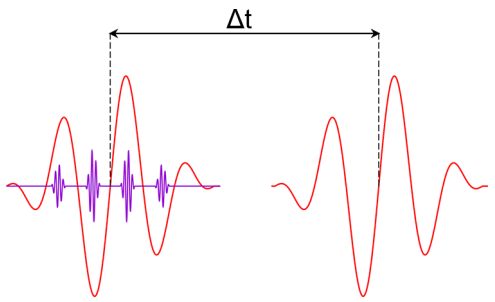

Figure 2. Pump−probe scheme. The pump is a phase-locked APT+IR combined field with attosecond pulses at the maxima of the IR field. The probe is another IR field, identical to the pump IR. The delay between them is defined with respect to the center of their envelopes. In the figure, the APT intensity is multiplied by 10^2 for clarity. The length of each IR field is three cycles (7.74 fs). All temporal envelopes are cosine-square functions.

The Born−Oppenheimer curves for the H_2 molecule are shown in Figure 1, together with the APT spectrum. Besides the H_2 $X^1\Sigma_g^+$ ground state, the figure shows the two first electronic states of the H_2^+ ion, $1s\sigma_g$ and $2p\sigma_u$. The first series of optically forbidden resonances $Q_1{}^1\Sigma_g^+$ is shown in red, and the first series of optically allowed resonances $Q_1{}^1\Sigma_u^+$ is shown in blue.

dx.doi.org/10.1021/jp3053136 | J. Phys. Chem. A XXXX, XXX, XXX−XXX

3. RESULTS

We will focus on the dissociative autoionization process $H_2^{**} \rightarrow H + H^+ + e^-$ and consider two observables, the electron kinetic energy (EKE) and the proton kinetic energy (PKE). Because we use a spectral method, we can remove at our will some states from the calculation and, hence, get physical insight about the electron and nuclear dynamics. This is not possible from a numerical solution of the TDSE, which in turn is more appropriate to describe ionization processes induced by intense laser pulses, but usually by reducing the dimensionality of the problem (see, e.g., ref 33 and references therein). To study the effect of the $Q_1\,^1\Sigma_g^+$ resonances, we will compare results from a calculation including all states and from a calculation in which those resonances are removed. We will also split the results into the possible final symmetries $^1\Sigma_g^+$ and $^1\Sigma_u^+$ imposed by the dipole selection rule for H_2 molecules parallel to the polarization direction of the (APT+IR)+IR field.

Single ionization from the H_2 molecule leads predominantly to vibrationally bound states in the $1s\sigma_g$ electronic state of the H_2^+ molecular ion. Most electrons in the EKE distributions come from this nondissociative channel. PKE spectra exclusively represent dissociative ionization, which is about 2 orders of magnitude smaller than nondissociative ionization but contains most of the autoionization signal. Therefore, it is in the PKE and not in the EKE where we will mainly observe the footprint of autoionization.

3.1. Photoelectron Spectra. The photoelectron spectrum as a function of time delay between the (APT+IR) pump and the IR probe is shown in Figure 3 (top). The probability at the left of the white vertical line corresponds to the case with no probe. The square of the vector potential is shown at the top of the figure, and the dashed horizontal lines indicate, for the different harmonic energies, the energy available for the electron when the system is in the $\nu = 2$ vibrational level of the $1s\sigma_g$ state of the H_2^+ ion (with $\nu = 3$, they are the most populated for all delays). These lines approximately indicate the EKE resulting form absorption of the different harmonics. Because higher (lower) vibrational levels are also populated, EKEs lying slightly below (above) these lines are also expected. As the probe IR pulse does not have enough intensity to induce photoionization or a significant electronic excitation in the molecule, the results corresponding to negative time delays (IR probe before the (APT+IR) pump) are very similar to those obtained without the IR probe.

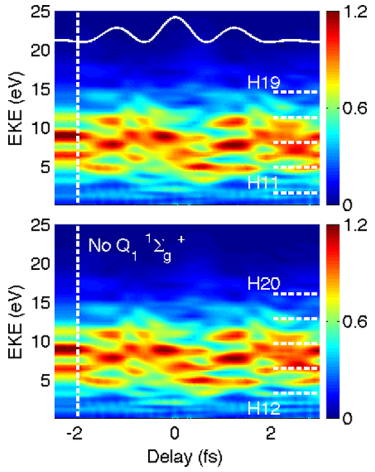

Figure 3. Photoelectron spectrum for the full calculation (top) and without the $Q_1\,^1\Sigma_g^+$ resonances (bottom). Results without the IR probe (only (APT+IR) pump) are shown at the left of the white vertical lines. The expected final energy upon absorption of a photon from each harmonic order is shown with horizontal lines. The square of the vector potential is shown in the upper part of the top figure. All probabilities are multiplied by 10^6.

There is an oscillation between bands (at odd harmonic orders) and sidebands (at even harmonic orders) as a function of the time delay, due to the interference between different harmonic orders: H17+ω and H19-ω, H17 + 2ω, and H19, etc. The periodicity of this oscillation is not clear in the pump−probe scheme used here, with two infrared fields. In the simpler case of an APT-pump-IR-probe scheme, there is a periodicity of $T/2$, where T is the infrared period.[29] Notice that, for the case with no probe, the maximum probability corresponds to the even harmonic orders, in the sidebands that result from XUV+IR absorption. This is the natural consequence of having designed an (APT+IR) pump in which the absorption of an IR photon is maximized by placing the attosecond pulses at the maxima of the IR field. The effect is clear in Figure 4, which shows the same results as Figure 3, but split into total symmetries $^1\Sigma_u^+$ (left) and $^1\Sigma_g^+$ (right). Again, results at the left of the vertical lines correspond to the case without the IR probe. The maximum probability corresponds to XUV+IR absorption ($^1\Sigma_g^+$) instead of to XUV one-photon absorption ($^1\Sigma_u^+$). The intensity of the different bands and sidebands in the EKE oscillate with time delay. Oscillations with $T/2$ periodicity, where $T = 2.58$ fs is the IR period, have been observed and explained in atoms[34−36] and molecules.[28,29] In the present case, the frequency of the oscillations is not so well-defined. As we will see below, this is the consequence of the presence of the two IR fields.

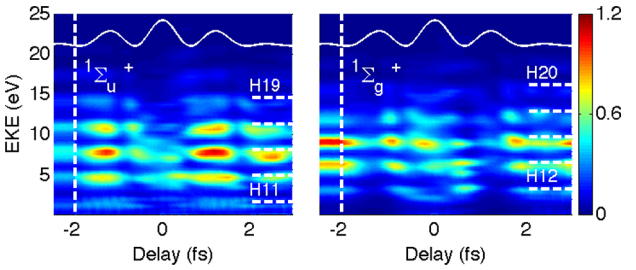

Figure 4. Same as in Figure 3, but split into total symmetry $^1\Sigma_u^+$ (left) and $^1\Sigma_g^+$ (right).

Figure 3 (bottom) shows the EKE spectrum obtained from a calculation in which the $Q_1\,^1\Sigma_g^+$ DESs have been removed. As can be seen, the spectrum is very similar to that shown in Figure 3 (top). Therefore, although the chosen scheme is very efficient in generating H_2 states of $^1\Sigma_g^+$ symmetry, autoionization is barely visible in the EKE spectrum. Small traces of this process are only observed at very small $|\Delta t|$, where small distortions with respect to the general oscillatory pattern are observed. As mentioned above, the minimum role played by autoionization in the EKE spectrum is due to the fact that nondissociative direct ionization is largely dominant.

3.2. Proton Kinetic Energy Spectra. The trace of autoionization is much better seen in the proton kinetic energy spectra. Figure 5 shows the result from the full calculation (top) and a calculation in which all the $Q_1\,^1\Sigma_g^+$ states have been removed (bottom), as a function of the time delay between the (APT+IR) pump and the IR probe. The intense band observed at low proton energies (≤1 eV) corresponds to direct dissociative

dx.doi.org/10.1021/jp3053136 | J. Phys. Chem. A XXXX, XXX, XXX−XXX

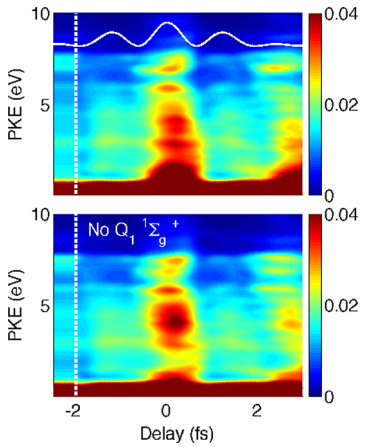

Figure 5. Proton kinetic energy spectrum for the full calculation (top) and without $Q_1{}^1\Sigma_g^+$ resonances (bottom). Results without the IR probe are shown to the left of the white vertical lines. The square of the vector potential is shown in the upper part of the top figure. All probabilities are multiplied by 10^6.

ionization through the H_2^+ $1s\sigma_g$ electronic state. At higher proton energies, the first noticeable feature is that the periodicity of the observed signal is approximately T. This is due to the presence of two identical IR fields, which add up constructively only after a whole period. In contrast, when a standard APT-pump/IR-probe scheme is used, the periodicity in the PKE spectra is $T/2$.[29] Results at the left of the vertical line correspond again to the case with no IR probe. There appears a higher population at proton energies $E \sim 7.75$ eV, which corresponds to direct dissociative ionization through the $2p\sigma_u$ channel, open within the Franck–Condon region for the harmonic H21.

An inspection of the dissociative ionization probability around zero time delay (central fringe in Figure 5) shows that, when the $Q_1{}^1\Sigma_g^+$ DESs are removed, there is a slightly enhanced population at medium PKE (~4 eV) and a noticeable depletion at low PKE (~1.5–2 eV). To understand these findings, we show in Figure 6 the same results split into total symmetries $^1\Sigma_u^+$ (left) and $^1\Sigma_g^+$ (right). When the $Q_1{}^1\Sigma_g^+$ states are not included (bottom figures), there is no possible transition to them from the lowest $Q_1{}^1\Sigma_u^+$ state via emission of an IR photon. As a consequence,

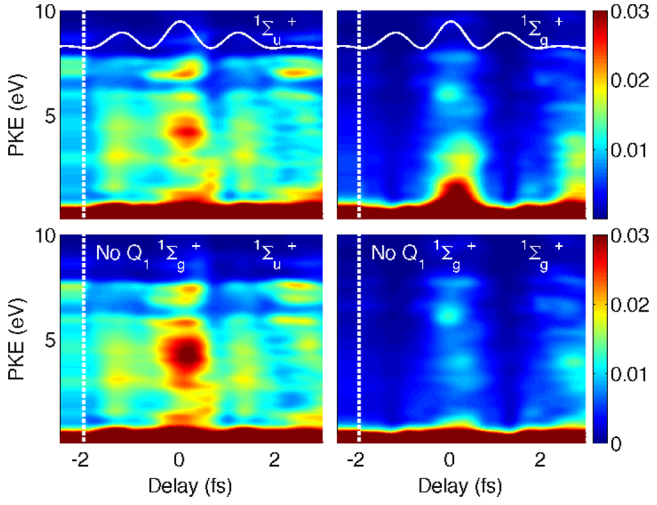

Figure 6. Same as in Figure 5, but split into total symmetry $^1\Sigma_u^+$ (left) and $^1\Sigma_g^+$ (right).

population of the lowest $Q_1{}^1\Sigma_u^+$ state is larger than in the presence of the $Q_1{}^1\Sigma_g^+$ states and autoionization into states of $^1\Sigma_u^+$ symmetry is more important. As the signature of autoionization from the $Q_1{}^1\Sigma_u^+$ states induced by photons of ~30 eV (i.e., those contained in the H19 harmonic) is more pronounced at a PKE of ~4–5 eV (see ref 25 and references therein), one thus expects an enhancement of the ionization probability in the $^1\Sigma_u^+$ channel around that energy. This explanation is confirmed by a comparison of the dissociative ionization probabilities shown in the two left panels of Figure 6 for this specific channel. Autoionization from the $Q_1{}^1\Sigma_g^+$ states, in turn, leads to very low-energy protons because the lifetime of these states is much shorter.[24,37] Therefore, when these resonances are removed, the dissociative ionization probability decreases significantly in the $^1\Sigma_g^+$ channel at low proton energies (see the comparison between the two right panels in Figure 6), hence in the total PKE spectrum (Figure 5).

The mechanisms by which the protons gain kinetic energy can be better understood from Figure 7. As the system evolves along

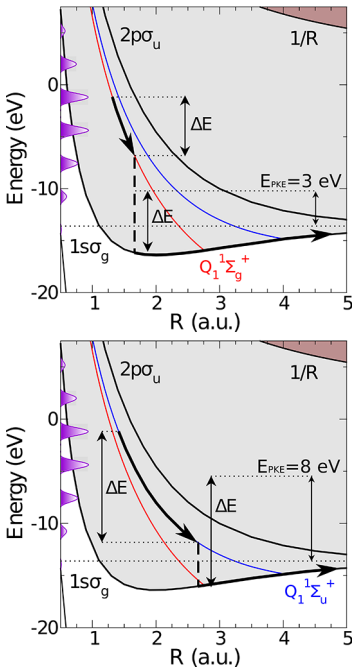

Figure 7. Nuclear kinetic energy gain through autoionization. The lowest two electronic states of H_2^+ (black curves), plus the $1Q_1{}^1\Sigma_g^+$ (red) and $1Q_1{}^1\Sigma_u^+$ (blue) DESs are shown. Autoionization from $1Q_1{}^1\Sigma_g^+$ is shown in the top figure, and autoionization from $1Q_1{}^1\Sigma_u^+$ in the bottom figure. Part of the energy gained by the nuclei before autoionization, ΔE, is used to overcome the dissociation threshold of H_2^+ and the remaining energy E_{pke} is transformed into kinetic energy that is shared between the nuclei (PKE = $E_{pke}/2$).

the potential energy curve of the lowest $Q_1{}^1\Sigma_g^+$ state (Figure 7, top), the nuclei gain a kinetic energy ΔE. When autoionization takes place, part of this energy must be used to overcome the ionization energy of H_2^+, leaving the nuclei with kinetic energy E_{pke} (where PKE = $E_{pke}/2$ for each nucleus). For $E_{pke} \sim 3$ eV as shown here, this leaves 1.5 eV per proton (low PKE feature in Figure 6, top right). The lowest $Q_1{}^1\Sigma_u^+$ DES has a much longer lifetime (a few femtoseconds), and therefore the nuclei can gain much more energy as the system evolves along the corresponding potential energy curve (Figure 7, bottom). This leads to higher excess energies. The excess energy of $E_{pke} = 8$ eV

dx.doi.org/10.1021/jp3053136 | J. Phys. Chem. A XXXX, XXX, XXX–XXX

shown here corresponds to protons detected at 4 eV in Figure 6, left.

The above results show not only that the pump−probe scheme used in the present work is very efficient in populating the lowest $Q_1{}^1\Sigma_g^+$ state but also that the latter state leaves a clear signature in the PKE at low energies. Nevertheless, the signature of this state is barely visible at time delays significantly larger than zero (e.g., in the region where the second fringe in the right-hand side of Figure 5 is seen). This is so because the lowest $Q_1{}^1\Sigma_g^+$ state has an extremely steep potential energy curve (Figure 1) and a very short lifetime, of ∼1 fs. Thus, its decay is so fast that it is practically completed within a period of the IR probe (∼2.58 fs). Hence the proposed scheme, which is based on what is available nowadays in the laboratory, is only useful to provide an upper bound of the autoionization lifetime of the short-lived $1Q_1{}^1\Sigma_g^+$ DES. To get deeper insight on its decay dynamics, one might try to probe the system by using pulses with a much faster period, e.g., a 200 nm UV probe. However, there are two objections to this: first, it is experimentally less complicated to achieve an (APT+IR)+IR setup than an (APT+IR)+UV one; second, the use of such big probe photons may lead to REMPI processes involving bound states of the $H_2{}^+$ molecule, which may hide the effect sought for.

4. CONCLUSIONS

We have studied the autoionization dynamics of the first series of optically forbidden doubly excited states of the H_2 molecule, the $Q_1{}^1\Sigma_g^+$ series. These states can be populated via two-photon absorption from the ground state of the molecule. For that purpose we use the simplest pump−probe scheme available with the current experimental techniques. The pump is a combined (APT+IR) field, containing phase-locked pulses, in which absorption of an APT photon is resonant with the lowest $Q_1{}^1\Sigma_u^+$ DES and emission of an IR photon is resonant with the lowest $Q_1{}^1\Sigma_g^+$ DES. An IR probe identical to the former IR pulse is used to track the autoionization dynamics by changing the time delay between the pump and the probe. We have solved the time-dependent Schrödinger equation by using a close-coupling method that accounts for all vibrational and electronic degrees of freedom for the case of H_2 molecules oriented parallel to the polarization direction of the laser. We have performed calculations both with all states included and without the $Q_1{}^1\Sigma_g^+$ resonances. From these calculations, we have found that the proton kinetic energy spectra (PKE) contain a clear signature of autoionization from both the lowest $Q_1{}^1\Sigma_g^+$ and $Q_1{}^1\Sigma_u^+$ states and exhibit a T periodicity due to the combination of the two IR fields. From the analysis of these PKE spectra with time delay one can easily see that the period of the IR probe is an upper bound of the autoionization lifetime of the lowest $Q_1{}^1\Sigma_g^+$ state. A more quantitative information about autoionization lifetimes should be obtained in systems where such lifetimes are significantly longer than the period of the IR pulses used in the present scheme.

AUTHOR INFORMATION

Corresponding Author

*E-mail: paula.riviere@uam.es.

Notes

The authors declare no competing financial interest.

ACKNOWLEDGMENTS

We gratefully acknowledge fruitful discussions with A. Palacios and A. González-Castrillo. This work was accomplished with an allocation of computer time from Mare Nostrum BSC and CCC-UAM. The research leading to these results has received funding from the European Union Seventh Framework Programme (FP7/2007-2013) under grant agreement No. 264951 and the European Research Council under the European Union's Seventh Framework Programme (FP7/2007-2013)/ERC grant agreement No. 290853, as well as MICINN Projects No. FIS2010-15127, No. ACI2008-0777, and No. CSD 2007-00010, the ERA-Chemistry Project No. PIM2010EEC-00751, and the European COST Action CM0702. R.E.F.S. acknowledges a Ph.D. contract from ITN CORINF. P.R. acknowledges a Juan de la Cierva contract grant from MICINN.

REFERENCES

(1) Scrinzi, A.; Ivanov, M. Y.; Kienberger, R.; Villeneuve, D. M. *J. Phys. B* **2006**, *39*, R1−R37.
(2) Krausz, F.; Ivanov, M. Y. *Rev. Mod. Phys.* **2009**, *81*, 163−234.
(3) Gopal, R.; et al. *Phys. Rev. Lett.* **2009**, *103*, 053001.
(4) Johnson, N. G.; et al. *Phys. Rev. A* **2011**, *83*, 013412.
(5) Sansone, G.; et al. *Nature* **2010**, *465*, 763−766.
(6) Sánchez, I.; Martín, F. *J. Chem. Phys.* **1997**, *107*, 8391.
(7) Sánchez, I.; Martín, F. *J. Chem. Phys.* **1999**, *110*, 6702.
(8) Drescher, M.; Hentschel, M.; Kienberger, R.; Uiberacker, M.; Yakovlev, V.; Scrinzi, A.; Westerwalbesloh, T.; Kleineberg, U.; Heinzmann, U.; Krausz, F. *Nature* **2002**, *419*, 803−7.
(9) Miaja-Avila, L.; Saathoff, G.; Mathias, S.; Yin, J.; La-o vorakiat, C.; Bauer, M.; Aeschlimann, M.; Murnane, M.; Kapteyn, H. *Phys. Rev. Lett.* **2008**, *101*, 046101.
(10) Tong, X. M.; Ranitovic, P.; Hogle, C.; Murnane, M.; Kapteyn, H.; Toshima, N. *Phys. Rev. A* **2011**, *84*, 013405.
(11) Ranitovic, P.; Tong, X. M.; Hogle, C.; Zhou, X.; Liu, Y.; Toshima, N.; Murnane, M.; Kapteyn, H. *Phys. Rev. Lett.* **2011**, *106*, 053002.
(12) Zherebtsov, S.; Wirth, a.; Uphues, T.; Znakovskaya, I.; Herrwerth, O.; Gagnon, J.; Korbman, M.; Yakovlev, V. S.; Vrakking, M. J. J.; Drescher, M.; et al. *J. Phys. B* **2011**, *44*, 105601.
(13) Sánchez, I.; Martín, F. *Phys. Rev. Lett.* **1997**, *79*, 1654.
(14) Martín, F. *J. Phys. B* **1999**, *32*, R197.
(15) Martín, F.; et al. *Science* **2007**, *315*, 629−33.
(16) Dowek, D.; Pérez-Torres, J. F.; Picard, Y. J.; Billaud, P.; Elkharrat, C.; Houver, J. C.; Sanz-Vicario, J. L.; Martín, F. *Phys. Rev. Lett.* **2010**, *104*, 233003.
(17) Palacios, A.; Bachau, H.; Martín, F. *Phys. Rev. Lett.* **2006**, *96*, 143001.
(18) Sanz-Vicario, J. L.; Bachau, H.; Martín, F. *Phys. Rev. A* **2006**, *73*, 033410.
(19) Palacios, A.; Bachau, H.; Martín, F. *Phys. Rev. A* **2007**, *75*, 013408.
(20) Fano, U. *Phys. Rev.* **1961**, *124*, 1866.
(21) Feshbach, H. *Ann. Phys.* **1962**, *19*, 287.
(22) Chesnel, J.-Y.; Martina, D.; Sobocinski, P.; Kamalou, O.; Frémont, F.; Fernández, J.; Martín, F. *Phys. Rev. A* **2004**, *70*, 010701(R).
(23) Tennyson, J. *At. Data Nucl. Data Tables* **1996**, *64*, 253.
(24) Sánchez, I.; Martín, F. *J. Chem. Phys.* **1997**, *106*, 7720.
(25) González-Castrillo, A.; Palacios, A.; Catoire, F.; Bachau, H.; Martín, F. *J. Phys. Chem. A* **2012**, *116*, 2704−2712.
(26) Pérez-Torres, J. F.; Morales, F.; Sanz-Vicario, J. L.; Martín, F. *Phys. Rev. A* **2009**, *80*, 011402(R).
(27) González-Castrillo, A.; Palacios, A.; Bachau, H.; Martín, F. *Phys. Rev. Lett.* **2012**, *108*, 063009.
(28) Kelkensberg, F.; Siu, W.; Pérez-Torres, J. F.; Morales, F.; Gademann, G.; Rouzée, A.; Johnsson, P.; Lucchini, M.; Calegari, F.; Sanz-Vicario, J. L.; et al. *Phys. Rev. Lett.* **2011**, *107*, 043002.
(29) Silva, R. E. F.; Rivière, P.; Martín, F. *Phys. Rev. A* **2012**, *85*, 063414.
(30) Ranitovic, P.; et al. *New J. Phys.* **2010**, *12*, 013008.
(31) Palacios, A.; Bachau, H.; Martín, F. *Phys. Rev. A* **2006**, *74*, 031402(R).
(32) Bachau, H.; Cormier, E.; Decleva, P.; Hansen, J. P.; Martín, F. *Rep. Prog. Phys.* **2001**, *64*, 1815−1942.

(33) Bandrauk, A. D.; Chelkowski, S.; Diestler, D.; Manz, J.; Yuan, K.-J. *Phys. Rev. A* **2009**, *79*, 023403.
(34) Johnsson, P.; Mauritsson, J.; Remetter, T.; L'Huillier, A.; Schafer, K. J. *Phys. Rev. Lett.* **2007**, *99*, 233001.
(35) Rivière, P.; Uhden, O.; Saalmann, U.; Rost, J. *New J. Phys.* **2009**, *11*, 053011.
(36) Tong, X. M.; Ranitovic, P.; Cocke, C. L.; Toshima, N. *Phys. Rev. A* **2010**, *81*, 021404(R).
(37) Pérez-Torres, J. F.; Sanz-Vicario, J. L.; Bachau, H.; Martín, F. *J. Phys. B* **2010**, *43*, 015204.